Theor Chem Acc (2002) 108:352–364
DOI 10.1007/s00214-002-0393-3

Theoretical
Chemistry Accounts

*Regular article*

# The reduction of ribonucleotides catalyzed by the enzyme ribonucleotide reductase

**Pedro Alexandrino Fernandes**[1], **Leif A. Eriksson**[2], **Maria João Ramos**[1]

[1]CEQUP/Faculdade de Ciências do Porto, Rua do Campo Alegre 687, 4169-007 Porto, Portugal
[2]Department of Biochemistry, Box 576, Uppsala University, 751 23 Uppsala, Sweden

Received: 5 August 2002 / Accepted: 30 September 2002 / Published online: 20 November 2002


**Abstract.** This work is devoted to the study of the radical catalytic pathway for the ribonucleotide reduction process assisted by ribonucleotide reductase. The present study is directed toward the investigation of one of the most controversial steps in the reduction pathway – the elimination of the 2′ hydroxyl group from the ribonucleotide. Several groups have made different proposals for this step, which all fit available experimental data; however, so far, it has not been possible to demonstrate clearly which is the correct pathway for the elimination. Here, we resort to high-level quantum mechanical calculations to analyze the energetics of the proposed mechanisms, as well as to propose alternative pathways, and evaluate their feasibility, according to the observed kinetics of the enzyme and other existing experimental data. Our study shows that the elimination occurs via two different simultaneous acid-/base-catalyzed pathways, depending on the protonation state of one key active site amino acid, Glu441.
**Electronic Supplementary Material.** Supplementary material is available for this article if you access the article at http: //dx.doi.org/10.1007/s00214-002-0393-3.

**Key words:** Ribonucleotide reductase – Reaction mechanism – Transition state – Density functional theory – Continuum

## 1 Introduction

Ribonucleotide reductases (RNRs) are fundamental enzymes in all living organisms. They catalyze the rate-limiting step in DNA biosynthesis, which consists of the reduction of ribonucleotides to 2′-deoxyribonucleotides [1, 2, 3, 4, 5, 6]. Therefore, they play an essential role in the regulation of cell growth and cell regeneration, and have recently become a promising target for the design of new chemical therapeutic agents, mainly in the field of antitumor and antiviral treatment [5, 7, 8, 9, 10]. Recent in vivo experiments on the inactivation of the enzyme have revealed potent antiproliferative effects against a wide range of tumor cell lines [10, 11, 12], as well as human xenografts in mice [10, 13, 14]. There are three classes of RNRs, according to the required cofactors necessary for catalytic activity. It is believed that all of them follow a radical mechanism to dehydrate the substrate. Class I RNRs possess a stable tyrosyl radical adjacent to a diiron cluster [15, 16]. Class II RNRs use AdoCbl as a cofactor [17, 18]. Class III RNRs are expressed in an anaerobic environment and possess a glycyl radical generated by an FeS cluster [19, 20]. A fourth class is proposed to exist only by one research group, with a protein radical (probably a tyrosyl radical) generated by a dimanganese cluster [21, 22, 23]. This study is devoted to Class I RNRs. This enzyme is an $\alpha_2\beta_2$ tetramer, constituted by two catalytically inactive homodimers [24]. The $\alpha_2$ dimer is called the R1 subunit and the $\beta_2$ dimer is called the R2 subunit. R1 has a molecular weight of 171 kDa and R2 a molecular weight of 87 kDa. The radical is generated in the R2 subunit, where a tyrosyl radical results from hydrogen abstraction by an oxo-bridged diiron center, located 30–40 Å from the active site. The radical is subsequently transmitted through a long chain of hydrogen-bonded amino acids, from Tyr122 near the diiron complex, to Cys439 at the active site in R1 [25]. The way the radical is transmitted to the active site is poorly understood at best. Both the radical formation at R2 and the way it is transmitted to the active site are subjects of intense investigation presently, and will not be addressed in the present work. Here we begin at the moment when the substrate is activated, i.e. loses a hydrogen atom to Cys439 and becomes a radical. The catalytic mechanism has been the subject of intense research in the last few decades, and several mechanistic proposals have been put forward [1, 3, 5, 26, 27, 28, 29, 30, 31, 32, 33]. One of the proposals,

Electronic Supplementary Material. Supplementary material is available for this article if you access the article at http: // dx.doi.org/10.1007/s00214-002-0393-3.

*Correspondence to*: M. J. Ramos
e-mail: mjramos@fc.up.pt

proposed by Stubbe and coworkers [1, 34, 35], postulated to be similar for all classes of RNRs, despite the drastically different cofactors required in each, is illustrated in Scheme 1. A recent theoretical proposal for the Class III RNR mechanism is indeed very similar to the mechanism of Class I RNR, and differences arise only in the step where carbon dioxide is formed [36].

After the transmission of the radical to the active site, the catalytic reaction proceeds by abstraction of the 3′-hydrogen atom from the substrate **1** by Cys439. A glutamate then abstracts a proton from the 3′ hydroxyl group of the nucleotide radical **2**, simultaneously with protonation of the 2′ hydroxyl group by Cys225, resulting in a water molecule and an α-keto radical **3**. Reduction of the α-keto radical by two active-site cysteine side chains yields the closed-shell derivative **4**, which is subsequently protonated by the active site glutamate, to yield the 3′-deoxyribonucleotide radical **5**. The final step consists of the abstraction of the hydrogen atom from Cys439, which leads to the formation of the reaction product **6** and regenerates the initial cysteine radical, which is subsequently retransmitted to Tyr122 in the R2 subunit.

Even though step 1 in Scheme 1 offers no controversy, step 2 has been the subject of several different proposals; therefore, we chose to begin our study at the 2′ hydroxyl elimination step. Besides the hypotheses illustrated in Scheme 1, several alternatives currently exist, both theoretical and experimental.

Lenz and Giese and [27] performed a series of competitive kinetic measurements for the dehydration of a photogenerated 3′ nucleoside radical in 1: 1 water/acetonitrile solvent. They measured the dependence of the dehydration rate on the pH, and on the concentration of the base catalyst (acetate). They concluded that the reaction was base-catalyzed, and should consist of two steps. The first evolves a hydrogen abstraction from the 3′ hydroxyl group by the base catalyst (here acetate), a slow, rate-determining step. The subsequent dehydration of the 2′ hydroxyl group will readily take place as a very fast step. On the basis of their results, a similar mechanism was proposed for RNR, using as base catalyst Glu441, an amino acid perfectly positioned to abstract the 3′ hydroxyl proton from the substrate (according to the recent X-ray structure of RNR with the bound substrate [37]).

Zipse proposed and Siegbahn studied theoretically a different mechanism for this step [31, 32, 38, 39]. Assuming that neutral models would mimic the active-site environment best, it was proposed that a protonated carboxylic group of the Glu441 side chain would form hydrogen bonds with the two hydroxyl groups of the substrate. It would act, therefore, as a bifunctional acid/base catalyst, protonating the 2′ hydroxyl group, and simultaneously abstracting the proton from the 3′ hydroxyl group. By resorting to quantum mechanical calculations, Siegbahn demonstrated that the energetics of that mechanism was coherent with the overall observed kinetics for the enzymatic reaction.

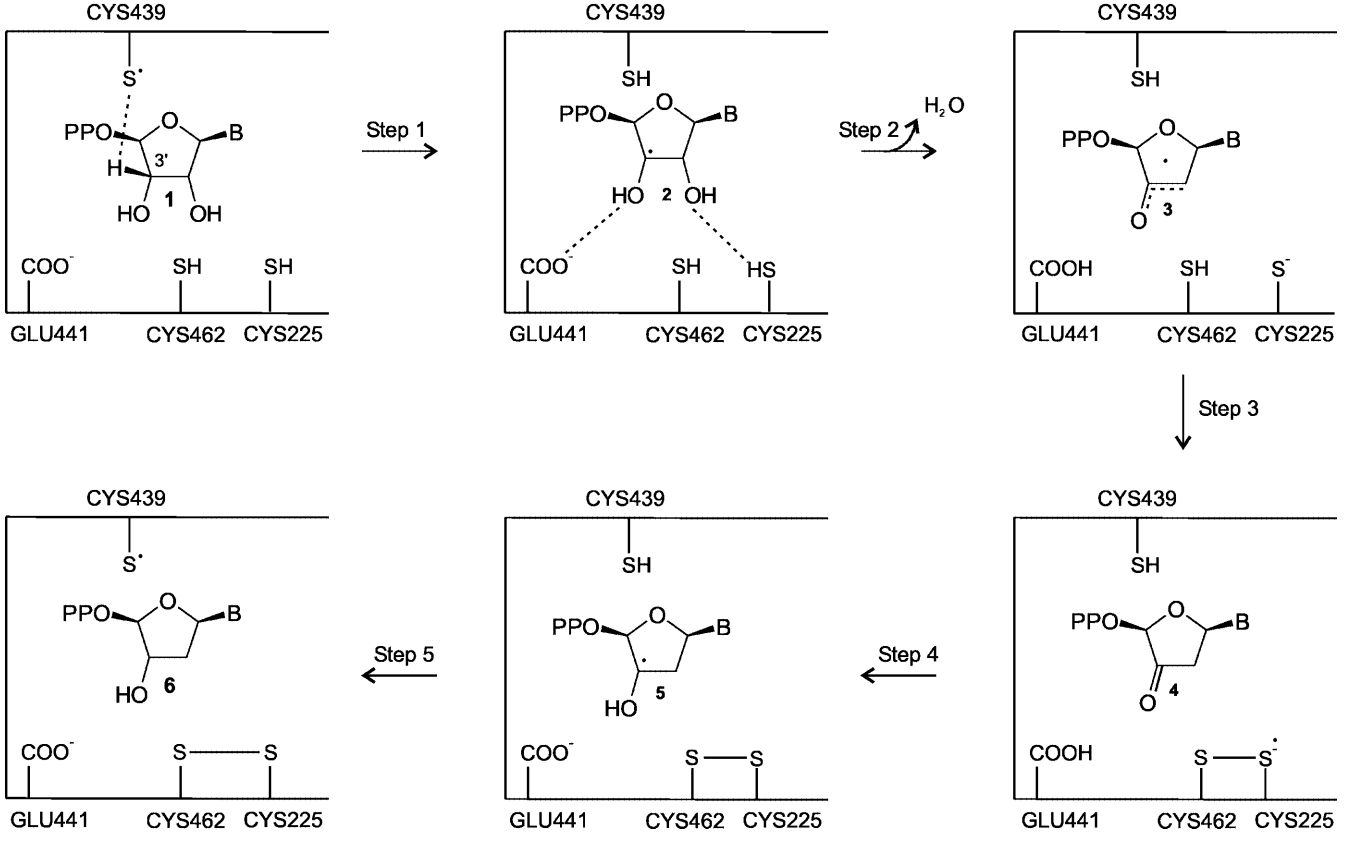


**Scheme 1.** Catalytic mechanism for the ribonucleotide reductase reduction of ribonucleotides into deoxyribonucleotides, postulated by Stubbe and van der Donk [1]

Acid-catalyzed mechanisms have also been proposed and should be accounted for, as protonation of the 2′ hydroxyl group would greatly facilitate subsequent dehydration. This is the case in, for example,, the acid-catalyzed dehydration of α,β-dihydroxyethane, which involves the formation of a radical cation [40]. As a result, intermediates such us a ribonucleotide radical with a protonated 2′ hydroxyl group, or a radical cation resulting from subsequent dehydration, could be formed [1, 3, 26, 28, 29, 32, 41, 42]. Acid catalysis was also considered for RNR in the early mechanisms proposed by Stubbe [3, 43], but was later replaced by the mechanism illustrated in Scheme 1.

Another hypothesis to be considered is an internal rearrangement, such as a 2→3 hydroxyl shift, followed by facilitated dehydration. Smith et al. [44] have studied extensively such coenzyme $B_{12}$ dependent rearrangements, and there is good evidence that a similar mechanism occurs in the dehydration of 1,2-dihydroxyethane catalyzed by the enzyme diol dehydratase [45], which catalyzes the dehydration of 1,2-dihydroxylethane into acetaldehyde via a radical mechanism [40, 46]. The similarities of that reaction with the RNR-catalyzed dehydration make us believe that such a possibility should also be considered.

The previously described mechanisms are all explored in the present work, through quantum chemical calculations in vacuum and in a continuum, to find out which are consistent with existing experimental data.

The article is organized as follows. A brief description of the methods employed in this work, as well as their virtues and limitations, is made in Sect. 2. The proposed mechanisms are analyzed in Sect. 3, and are compared with the available experimental data. The conclusions of this work are collected in Sect. 4, in which the implications in the present knowledge of the enzyme-assisted dehydration of ribonucleotides are discussed.

## 2 Methods

All the calculations were performed at the Becke3LYP level of theory [47, 48, 49]. Three different basis sets were employed, namely 6-31G(d), 6-311+G(2d,p) and 6-311++G(3df,3pd). Throughout this work they are termed medium basis (MB), large basis (LB) and very large basis (VLB), respectively. In geometry optimizations the MB was used. It is well known that larger basis sets give very small additional corrections to the geometries, and are hence considered unnecessary from a computational viewpoint [25, 31, 50]. However, the larger basis sets were used to calculate the energies of the optimized geometries. For this purpose we used the triple-ζ quality LB and VLB. According to the results, the VLB basis set seems to be very close to saturation in the present system. Frequency analysis was performed at each stationary point on the potential-energy surface. All minima and transition states were identified by the number of imaginary frequencies. Thereafter the transition states were verified to connect the reactants and products of interest through internal reaction coordinate calculations. A scaling factor of 0.9468 was used for the frequencies. Zero-point and thermal effects (298.15 K, 1 bar) were added to the calculated energies, and were also analyzed separately.

In the gas phase, hydrogen-bonded complexes always have a large number of conformers. The conformers presented in the schemes and figures were chosen so as to mimic, as closely as possible, the geometry of the active site. The isomers of the ribose ring are the same as in the natural substrate. It was previously suggested that the use of neutral models leads to better convergence in the calculations [51], and could eventually result in better agreement with experimental data, avoiding artifacts due to the use of charged species [52]. In the present work some of the models were chosen to be charged, since some of the reaction mechanisms are ionic in nature and could not be replaced by neutral analogues. Artifacts could appear if residues in the enzyme that stabilize the charged species were neglected from the models, which was not the case here.

As our models include charged species, it is crucial to understand the importance of long-range effects on the energetics of the reaction. To this end we used a polarized continuum model, referred to as C-PCM, as implemented in Gaussian98 [53]. In this approximation, the continuum is modeled as a conductor, instead of a dielectric. This simplifies the electrostatic computations, and corrections are made a posteriori for dielectric behavior. According to previous studies on active sites in proteins, an empirical dielectric constant of 4 gives good agreement with experimental results, and accounts for the average effect of both the protein and the buried water molecules [25, 31, 54].

When performing calculations with a macroscopic continuum model, it is usually assumed that gas-phase geometries and zero-point energies can be transferred without introducing any significant error. However, owing to the charged nature of several models, in the present work all steps were performed under the influence of the dielectric continuum. First, the geometries were reoptimized and frequencies, zero-point and thermal effects were estimated under the dielectric continuum. The energies were then recalculated using the larger basis sets. In general, the effect of the continuum was found to be small for both geometries and energies, even in the charged systems.

In open-shell systems, spin contamination is a frequent problem. It is well known that density functional theory methods are quite robust to spin contamination, and in the calculations presented here, the expectation value for $S^2$ never reached a value above 0.76, before correction. Atomic-charge and spin-density distributions were calculated with a Mulliken population analysis [55], using the larger basis sets. All the calculations were performed with the Gaussian98 suite of programs [53].

## 3 Results

### *3.1 Base catalysis by Glu441*

According to the experiments of Lenz and Giese [27], the first step should be a hydrogen abstraction from the 3′ hydroxyl group followed by fast elimination of the 2′ hydroxyl group, as depicted by reactions 1a–c in Scheme 2, where a ribose molecule models the substrate, a formate ion models a glutamate side chain and a methylthiol molecule models a cysteine side chain.

In reactions 1b and c we depict the two possible proton donors for this step, the thiol of Cys225 and the glutamate of Glu441, protonated in the earlier step (reaction 1a).

We studied both mechanistic steps independently, and the activation energies and reaction enthalpies of the overall process are shown in Scheme 3. The transition state for reaction 1a is illustrated in Fig. 1.

At the transition state, the abstracted hydrogen makes two long hydrogen bonds with the 2′ and 3′ hydroxyl oxygens of the substrate, with lengths of 1.985 and 2.276 Å, respectively, and can be classified as a late transition state. In the reactants, the hydrogen bonds between the glutamate oxygen and the two hydroxyl groups are shorter, with lengths of 1.792 and 1.608 Å, respectively. In the products there is only one hydrogen bond, a strong, short hydrogen bond formed between the 2′ oxygen and

REACTION 1a

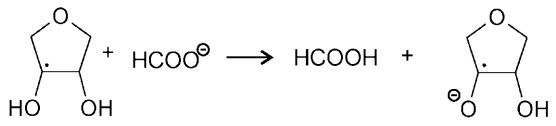

REACTIONS 1b and 1c

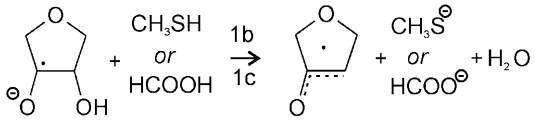

REACTION 2

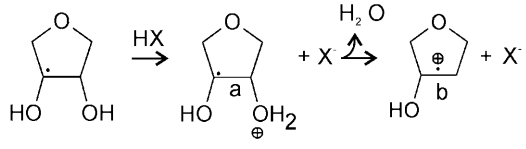

REACTION 3a

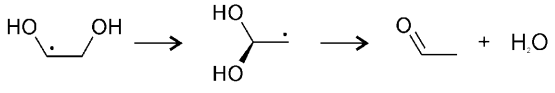

REACTION 3b

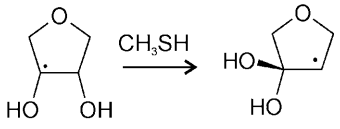

REACTION 4a

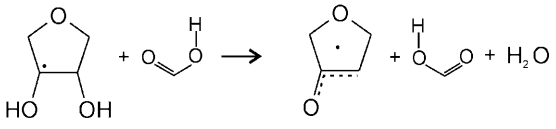

REACTON 4b

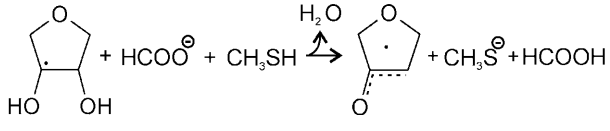

**Scheme 2.** Chemical reactions

the abstracted hydrogen, with a length of 1.528 Å. The spin density does not change much during the course of the reaction. There is a tendency for the spin density to increase at the 3′ carbon (0.88 a.u. in the reactants, 0.92 a.u. in the transition state and 0.98 a.u. in the products). The 3′ oxygen also has a considerable spin density (0.13 a.u. in the reactants, 0.24 a.u. in the transition state and 0.23 a.u. in the products).

The activation energy is 22.6 kcal $mol^{-1}$ and the enthalpy of reaction is 14.9 kcal $mol^{-1}$. Zero-point and thermal effects reduce the reaction barrier by 0.2 kcal $mol^{-1}$ and the reaction enthalpy by 0.8 kcal $mol^{-1}$. The long-range polarization does not change the activation energy within the accuracy of the calculation; however, it increases the reaction enthalpy by 0.7 kcal $mol^{-1}$. By comparing the gas-phase and protein-medium optimized geometries, we conclude that the geometry changes are negligible. The differences of zero-point and thermal energies in the gas phase and within the protein are also small, corresponding to an increase of 0.7 kcal $mol^{-1}$ in both the activation energy and the reaction enthalpy. At the transition state, the negative charge has already been transferred from the glutamate to the substrate.

After the first step, dehydration proceeds via 2′ hydroxyl elimination. This step can be facilitated by protonation by an acidic group. Reaction 1b models the protonation of the hydroxyl group by the side chain thiol group of one of the active-site cysteines (probably Cys225), and by the protonated thiolate (from Glu441), followed by dehydration. We will discuss primarily the protonation by the thiol group.

The transition state for reaction 1b is illustrated in Fig. 1b. This is an early transition state as the 2′ hydroxyl group is already leaving the ribonucleotide (C–O distance of 1.863 Å in the transition state and 1.493 Å in the reactants), although the thiol S–H bond remains only slightly extended (1.428 Å at the transition state versus 1.370 Å in the reactants). The hydrogen bond between the hydroxyl and thiol groups is shortened significantly at the transition state (1.628 Å at the transition state and 1.918 Å in the reactants). The spin density shifts toward the sulfur atom, from the reactants to the products. In the reactants, the spin density is mainly distributed between the 3′ oxygen (0.27 a.u.) and the 3′ carbon (0.74 a.u.). At the transition state the spin density delocalizes to the leaving 2′ HO group, with values of 0.26 a.u. at the 3′ oxygen, 0.25 a.u. at the 3′ carbon, 0.32 a.u. at the 2′ carbon and 0.18 a.u. at the 2′ oxygen. In the reaction products, the spin density remains mostly localized at the sulfur atom (spin densities of 0.47 a.u. at the sulfur, 0.18 a.u. at both the 2′ and 3′ carbons and 0.14 a.u. at the 3′ oxygen).

Analysis of the charge distribution elucidates that the ribonucleotide radical retains the negative charge in the reactants and transition state (−0.97 and −0.95 a.u., respectively); however, in the product the negative charge is delocalized between the cysteine residue and the 2′-deoxy-3′-ketonucleotide moiety (−0.54 a.u. in the cysteine and −0.44 a.u. in the ketonucleotide).

From these data it is not clear where the radical will be localized at the end of the reaction. However, by

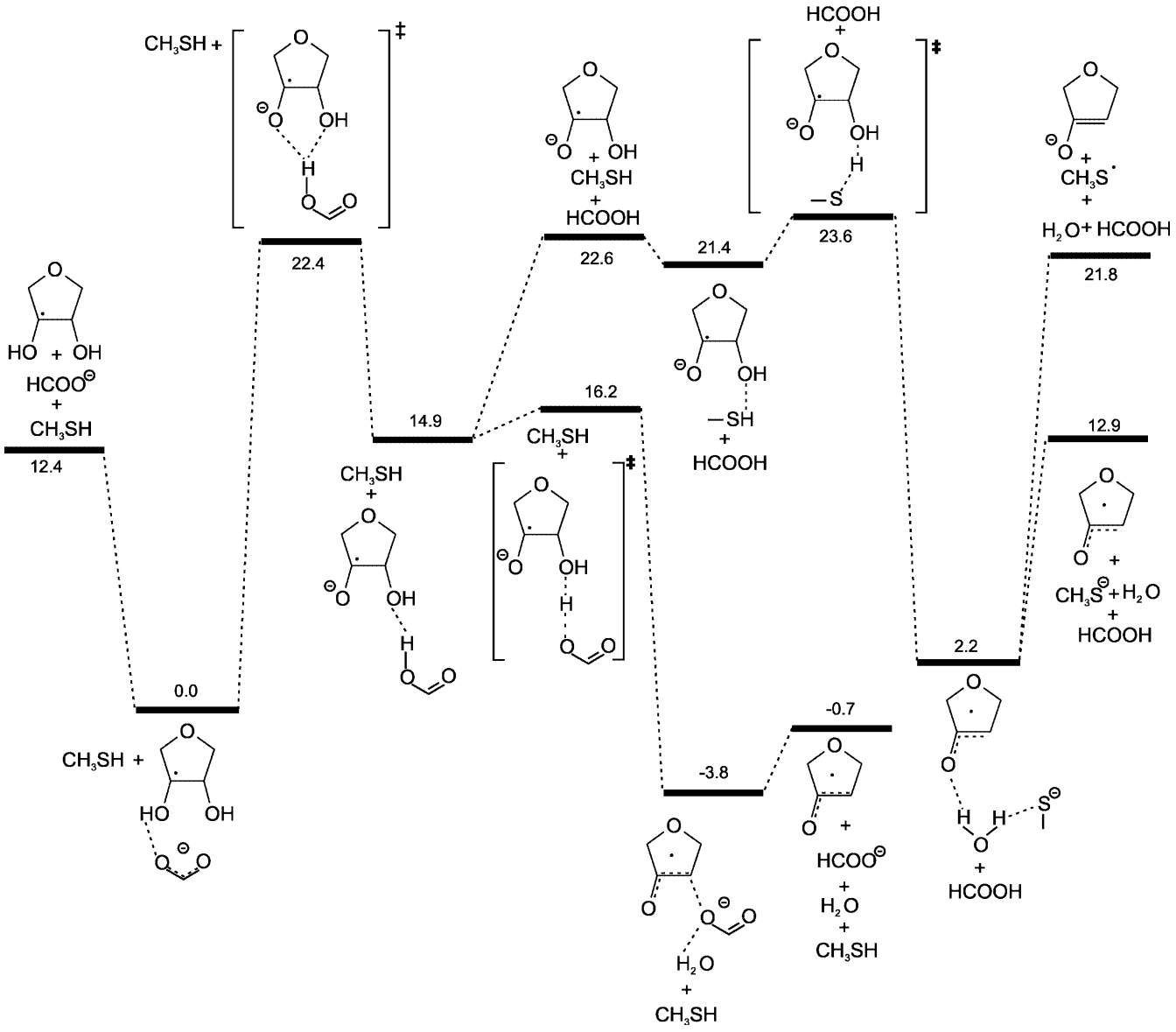


**Scheme 3.** Activation energies and reaction enthalpies for reactions 1a, b and c. All energies in kcal $mol^{-1}$

calculating the difference between the energies of the monomers that participate in the reaction, we have concluded that placing the radical at the 2′-deoxy-3′-ketonucleotide moiety residue, and the negative charge at the cysteine thiolate, results in a larger stabilization (by 8.9 kcal $mol^{-1}$) than placing the radical in the opposite species. We conclude, therefore, that the radical becomes localized at the 2′-deoxy-3′-ketonucleotide moiety at the end of the reaction, and that the cysteine will retain a negative charge.

The reaction has an activation energy of 2.1 kcal $mol^{-1}$ and a reaction enthalpy of −21.4 kcal $mol^{-1}$. Zero-point and thermal corrections account for a decrease of 1.7 kcal $mol^{-1}$ in the activation energy and an increase of 1.0 kcal $mol^{-1}$ in the reaction enthalpy. The long-range polarization only accounts for an increase of 0.1 kcal $mol^{-1}$ in the reaction barrier and 0.3 kcal $mol^{-1}$ in the reaction enthalpy. Geometry changes induced by the dielectric medium are again very small, mainly a shortening of the thiol–hydroxyl hydrogen bond of 0.038 Å in the reactants and 0.042 Å in the transition state. Consequently, at the transition state, the C3–O3 bond length increases by 0.028 Å in the dielectric medium.

The other mechanistic alternative corresponds to the protonation of the 2′ hydroxyl group by the carboxylate of Glu441. This can be achieved directly from the products of reaction 1a. The transition state for such protonation is illustrated in Fig. 1c.

This is an even earlier transition state. The 3′ C–3′ O bond length is 1.432 Å in the reactants, and at the transition state is stretched to only 1.592 Å. The H–O bond of the acidic hydrogen is only slightly stretched to 1.060 Å (compared with 1.055 Å in the reactants). The hydrogen bond between the proton from Glu441 and the leaving HO group has a length of 1.489 Å.

The spin density at the transition state is distributed between the 3′ oxygen (0.26 a.u.) and the 3′ carbon

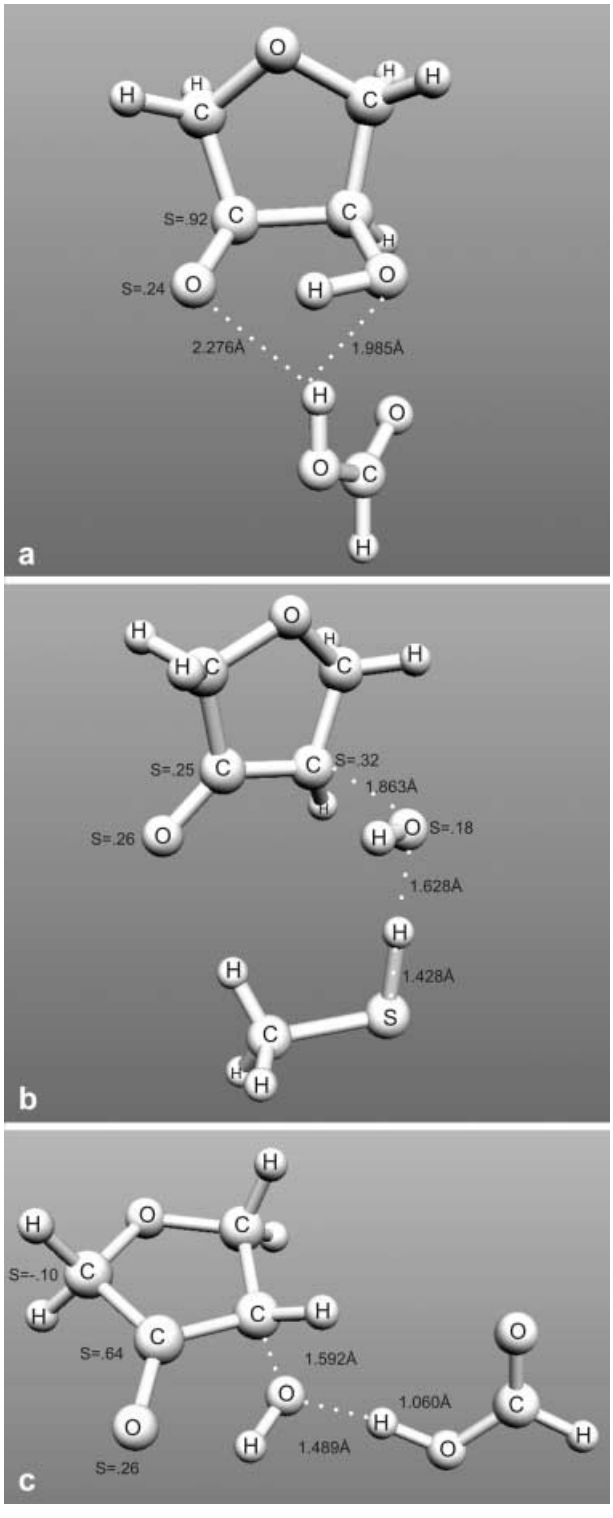


**Fig. 1.** Optimized transition-state geometries for **a** reaction 1a, **b** reaction 1b and **c** reaction 1c. Relevant distances (Å) and *spin densities* (a.u.) are indicated

(0.64 a.u.). After dehydration, this distribution changes significantly, and in the products the spin density is mainly distributed between the 2′ carbon (0.81 a.u.) and the 3′ oxygen (0.27 a.u.).

Analysis of the charge distribution at the transition state allows us to conclude that the leaving OH group carries a significant fraction of the negative charge (−0.66 a.u.). The activation energy for this reaction is only 1.3 kcal $mol^{-1}$. The reaction is exothermic by 20.0 kcal $mol^{-1}$. Zero-point and thermal effects account for a decrease of 1.1 kcal $mol^{-1}$ in the activation energy and 0.2 kcal $mol^{-1}$ in the reaction enthalpy. The effect of the dielectric continuum is very small, only a decrease of 0.7 kcal $mol^{-1}$ in the activation energy and an increase of 1.4 kcal $mol^{-1}$ in the enthalpy of reaction. The very low activation energy for this step shows that it is to be preferred over the protonation by the thiol group (reaction 1b).

The kinetics for the wild-type Class I RNR from *Escherichia coli* give $K_{cat} = 3.1\ s^{-1}$ [56] (the highest value for $K_{cat}$ for Class I RNR is around 10 $s^{-1}$). As this step is not rate-limiting in the catalytic mechanism, any mechanistic step with an activation energy close to 17 kcal $mol^{-1}$ should be ruled out. We thus conclude that although the proposed mechanism behaves qualitatively as expected (i.e. a slow first step followed by fast HO elimination [27]) the initial step does not match the experimental reaction kinetics, and should be excluded. It must be emphasized that the experiments of Lenz and Giese were performed in 1: 1 water/acetonitrile solvent, which results in a very different environment from the one experienced in the enzyme. It is well known that differential stabilization of the transition state by the solvent can lower reaction barriers in solution relative to gas-phase or enzymatic environments. Another explanation could be that the real mechanism in solution is different from that proposed by Lenz and Giese. As will be seen later, simultaneous acid- and base-catalyzed mechanisms are always preferred over their stepwise analogues. Hence, the reaction in solution could also be simultaneously acid- and base-catalyzed. A mechanism that would match the experimental observation of rate acceleration with increasing pH and with increasing concentration of base catalyst could involve hydrogen abstraction by the base catalyst simultaneously with the protonation of the 2′ hydroxyl group by a solvent water molecule. Such a concerted mechanism would exhibit base-catalyzed characteristics, (i.e. increasing rate with both increasing base concentration and pH) as the acid catalyst is the solvent and is in large excess.

In summary, a different mechanism than the base catalysis by Glu441 must exist in order to explain the observed kinetics of the RNR dehydration reaction.

### *3.2 Acid catalysis*

An acid-catalyzed mechanism, as proposed by several authors, would need a strongly acidic residue with access to the 2′ HO group. Moreover, a protonated radical **a** and a carbocation **b**, as illustrated in reaction 2, should then occur as intermediaries in the dehydration step [1, 3, 26, 28, 29, 32, 41, 42].

Studies performed by us revealed that the protonated radical **a** is not a minimum on the potential-energy surface at the UB3LYP/MB//UB3LYP/MB level of theory, and decomposes without activation into the

carbocation **b** and a hydrogen-bonded water molecule. A potential-energy surface scan along the C2–O2 bond is shown in Fig. 2.

The energetics of the hydrated radical cation lies clearly above that of the dissociated counterpart. Similar results have been obtained in other model systems. Zipse and Mohr [32, 57] studied the addition of water to radical carbocations. The conclusions were that the addition of water to the radical carbocations does not lead to a minimum on the potential-energy surface, if the radical cation is already stabilized by carbon substituents. Instead, the hydrated species will readily dissociate into a hydrogen-bonded complex between a water molecule and a radical carbocation [32]. Therefore, if protonation of the 2′ HO group is feasible, dehydration will readily occur.

Initially, Stubbe [41] proposed that a thiol group from an active-site cysteine protonates the 2′ oxygen; however, such a situation seems very unlikely, since the $pK_a$ for the cysteine thiol group in a protein environment is around 9.0 [58] (unless the thiol or the thiolate is stabilized specifically through strong interactions, which is not the case at the RNR active site). The thiol group seems thus not to be acidic enough to protonate the hydroxyl group at an acceptable rate. Moreover, theoretical calculations on such protonation, using a slightly lower theoretical level than the one presently employed, led to an activation barrier for the simultaneous protonation/dehydration process of 16.2 kcal $mol^{-1}$, a value too high to be feasible [31]. As there is no other group at the active site acidic enough to efficiently protonate the 2′ oxygen at an acceptable rate, the acid catalysis hypothesis is excluded.

### *3.3 2→3 hydroxyl shift, followed by facilitated dehydration*

A third hypothesis is that an internal rearrangement could occur prior to dehydration. An example of such a process is the dehydration of ethane-1,2-diol into acethaldeyde and water, catalyzed by the enzyme diol dehydratase. Studies over the last 30 years have suggested that the reaction is initiated by abstraction of a hydrogen atom from the substrate, which would lead to the formation of the 1,2-dihydroxyeth-1-yl radical. The radical will then rearrange to the *gem*-diol form, and water elimination would generate the formylmethyl radical. Subsequent hydrogen abstraction would lead to the formation of acethaldeyde and to the regeneration of the original radical cofactor [46].

In this reaction, the hydroxyl shift is the rate-limiting step. Once formed, dehydration would readily occur. The analogy of the diol dehydrase catalytic dehydration with the reaction studied here made us investigate this possibility as well. Previous studies by Smith et al. [45, 59] indicate that a proton donor lowers the barrier for the 1,2-hydroxyl shift. In reaction 3b we used one of the active-site cysteines to facilitate the breaking of the 2′ C–O bond.

As protonation proceeds, the C–O bond length increases. However, if the catalyst lies in a correct orientation, the hydroxyl group does not leave the ribonucleotide (as in the preceding acid-catalyzed case). Instead, it turns to the 3′ carbon direction and converges to a transition state connecting the two minima in reaction 3b. The geometry of the transition-state is depicted in Fig. 3 and the activation energies and reaction enthalpies for the reaction are illustrated in Scheme 4.

In the reactants, the sulfur and hydrogen atoms of the cysteine thiol group make two long hydrogen bonds with the 3′ and 2′ hydroxyl groups of the substrate, with lengths of 2.319 and 2.076 Å, respectively. At the transition state the 2′ hydroxyl group is placed very close to the middle of the 2′–3′ C–C bond, and above the plane of the ring. The distances between the leaving 2′ oxygen and the 2′ and 3′ carbons correspond to 2.367 and 2.273 Å, respectively. The thiol group forms a much shorter hydrogen bond with the leaving 2′ hydroxyl group, with a length of 1.887 Å. In the products the

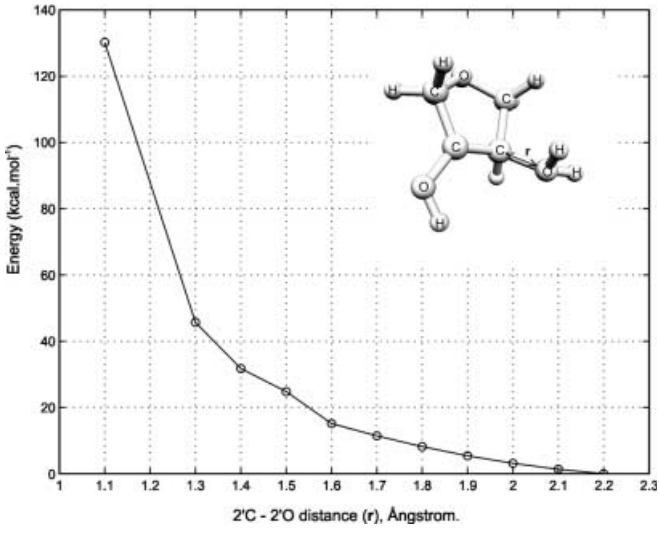


**Fig. 2.** Potential-energy surface for the dehydration of a radical cation intermediary

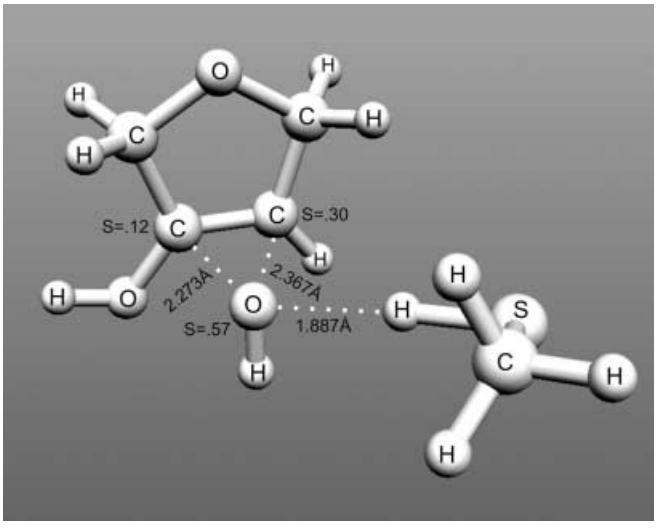


**Fig. 3.** Optimized geometry of the transition state for the 2→3 hydroxyl shift. Relevant *distances* (Å) and *spin densities* (a.u.) are indicated

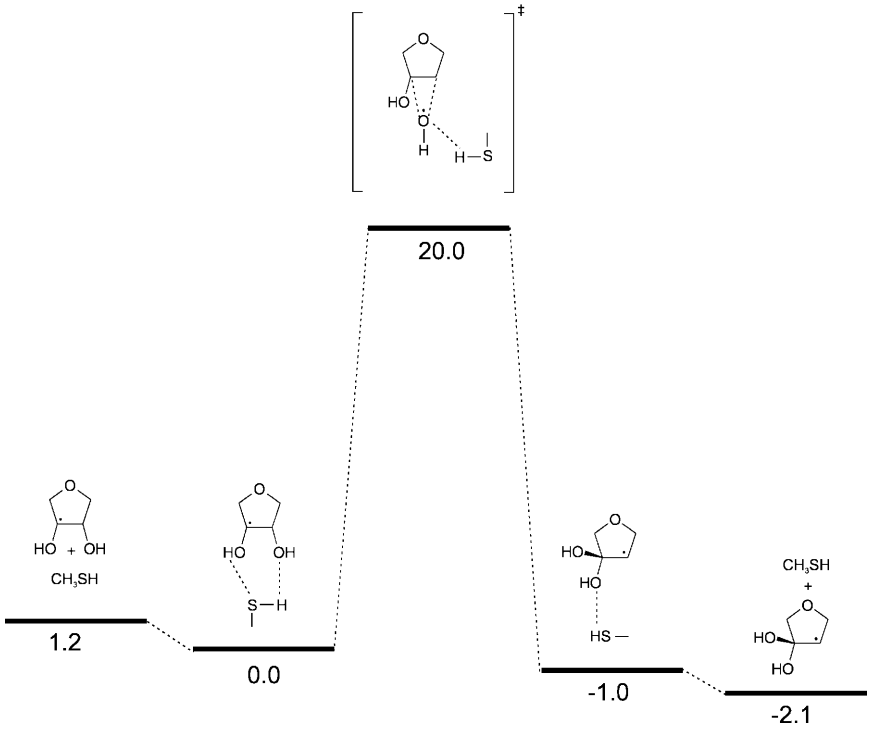


**Scheme 4.** Activation energies and reaction enthalpies for the hydroxyl shift from carbon 2 to carbon 3. All values in kcal $mol^{-1}$

hydroxyl group adds to the 3′ carbon. The hydrogen bond between this group and the thiol group is again much longer, with a length of 2.156 Å.

In the reactants, the spin density is mainly distributed between the 3′ carbon (0.89 a.u.) and the 3′ oxygen (0.12 a.u.). At the transition state, the spin density becomes delocalized to the oxygen of the leaving 2′ hydroxyl group, with a value of 0.57 a.u., and to the 2′ and 3′ carbon atoms (0.30 and 0.12 a.u., respectively). After the reaction, the spin density is mostly localized at the 2′ carbon (1.07 a.u.). A consequence of the shift of the 2′ hydroxyl group to the 3′ carbon is that the spin density shifts from the 3′ carbon to the 2′ carbon. The most significant changes in the geometry of the reactants induced by the dielectric continuum correspond to a shortening of 0.045 and 0.065 Å in the hydrogen bonds between the 3′ and 2′ hydroxyl groups and the thiol group, respectively. The geometric changes at the transition state are more substantial and result in the leaving hydroxyl group being shifted toward the 3′ carbon in the dielectric medium and toward the 2′ carbon in the gaseous phase. The distance between the leaving hydroxyl oxygen and the 3′ carbon is reduced by the continuum by 0.14 Å. Coherently, the distance between the leaving hydroxyl group and the 2′ carbons increases by 0.076 Å in the continuum.

The activation energy for this reaction corresponds to 20.0 kcal $mol^{-1}$ and the reaction enthalpy to −1.0 kcal $mol^{-1}$. The reaction is almost thermoneutral, as expected, since the chemical bonds broken and formed are similar. Zero-point and thermal effects amount to 2.1 kcal $mol^{-1}$ for the activation energy and −1.0 kcal $mol^{-1}$ for the reaction enthalpy. The effect of the dielectric continuum corresponds to a decrease of 2.9 kcal $mol^{-1}$ in the activation energy and of 1.3 kcal $mol^{-1}$ in the reaction enthalpy.

Similar theoretical results were found in the dehydration of the 1,2-dihydroxyeth-1-yl radical. The calculated activation energy for the transfer of the 2 hydroxyl group was 28.6 kcal $mol^{-1}$ [46].

In that case the proposed pathway involved protonation of the 2 hydroxyl group that dehydrates spontaneously into water and the *anti*-vinyl alcohol radical cation [46]. Smith et al. [44, p. 207] demonstrated that even a partial protonation leads to a decrease in the activation energy. In the present case, the distance between the acidic hydrogen and the migrating hydroxyl group at the transition state (1.887 Å), although smaller than in the reactants and products, is very large and can be classified as a very small partial protonation, thus implying only a very low decrease in the barrier. In the active site of RNR there is no residue capable of protonating the migrating hydroxyl more efficiently, as demonstrated in Sect. 3.2. On the basis of the observed kinetics for the enzyme, and considering the high activation energy (20.0 kcal $mol^{-1}$), we can conclude that the 2→3 hydroxyl shift occurs too slowly to match the RNR catalytic rate. The subsequent step (the *gem*-diol dehydration) was not studied, since the *gem*-diol cannot be present in the normal catalytic pathway.

### *3.4 Simultaneous acid/base catalysis*

In this category two different mechanisms will be explored. The first was originally proposed by Zipse [32] and was studied by Siegbahn [31] using theoretical methods. The second is a revised version of the acid-

catalyzed mechanism initially postulated by Stubbe and van der Donk [1]. The first reaction assumes the existence of a protonated glutamate residue at the active site, acting as a bifunctional catalyst. In the reactants, the glutamate side chain forms hydrogen bonds with the 3′ and 2′ hydroxyl groups of the substrate, with lengths of 1.748 and 1.622 Å, respectively. The catalyst then protonates the 2′ HO group and simultaneously abstracts a proton from the 3′ hydroxyl group. Protonation and dehydration of the 2′ hydroxyl group occur simultaneously, in agreement with the previous finding that a protonated hydroxyl group bonded to the substrate does not correspond to a minimum on the potential-energy surface. This reaction can be seen as a 2→3 hydrogen shift, catalyzed by the protonated glutamate. The optimized transition state for this reaction is illustrated in Fig. 4a. The hydrogen bond between the glutamate and the 3′ hydroxyl group is much shorter than in the reactants, and now corresponds to 1.499 Å. The 2′ hydroxyl group is being protonated by the acidic hydrogen of the glutamate, which is almost midway between the proton donor and acceptor (distances of 1.329 and 1.118 Å, respectively). Simultaneously, the 2′ hydroxyl group is leaving the ribonucleotide radical, with a C–O distance of 1.825 Å.

The spin density in the reactants is mainly distributed between the 3′ carbon (0.87 a.u.) and the 3′ oxygen (0.13 a.u.). At the transition state, the spin density is more delocalized toward the 2′ carbon, with values of 0.47 a.u. in the 3′ carbon, 0.16 a.u. in the 3′ oxygen, 0.22 a.u. in the 2′ carbon and 0.13 a.u. in the leaving 2′ oxygen. After the reaction, the spin density becomes mostly localized at the 2′ carbon (0.78 a.u.), although some spin density also remains at the 3′ oxygen (0.26 a.u.). Changes in the geometry of the reactants induced by the dielectric continuum correspond to a shortening of 0.029 and 0.047 Å in the hydrogen bonds between the 3′ and 2′ hydroxyl groups and the glutamate, respectively. The geometric changes at the transition state are mainly a shortening by 0.068 Å of the 2′ C–O distance, and minor changes at the hydrogen-bonding network.

The recent X-ray structure of RNR with the bound substrate [37] shows, however, that Glu441 is not at the optimal position to perform such a hydrogen transfer. It forms only one hydrogen bond with the 3′ hydroxyl group, although it is possible that an internal rearrangement would place the glutamate in a productive orientation.

The activation energies and reaction enthalpies for this reaction are depicted in Scheme 5a. The activation energy for this reaction corresponds to 4.6 kcal $mol^{-1}$ and the reaction enthalpy is −9.4 kcal $mol^{-1}$. Zero-point and thermal effects amount to −3.6 kcal $mol^{-1}$ for the activation energy and −0.8 kcal $mol^{-1}$ for the reaction enthalpy. Siegbahn showed that the inclusion of further active-site amino acids in the calculation could lower the activation energy even further. The effect of the dielectric continuum corresponds to a decrease of 1.2 kcal $mol^{-1}$ in the activation energy and an increase of 0.9 kcal $mol^{-1}$ in the reaction enthalpy. Although this straightforward, low barrier mechanism seems to be perfectly suited for RNR, it does suffer from a severe constraint, i.e. the initial

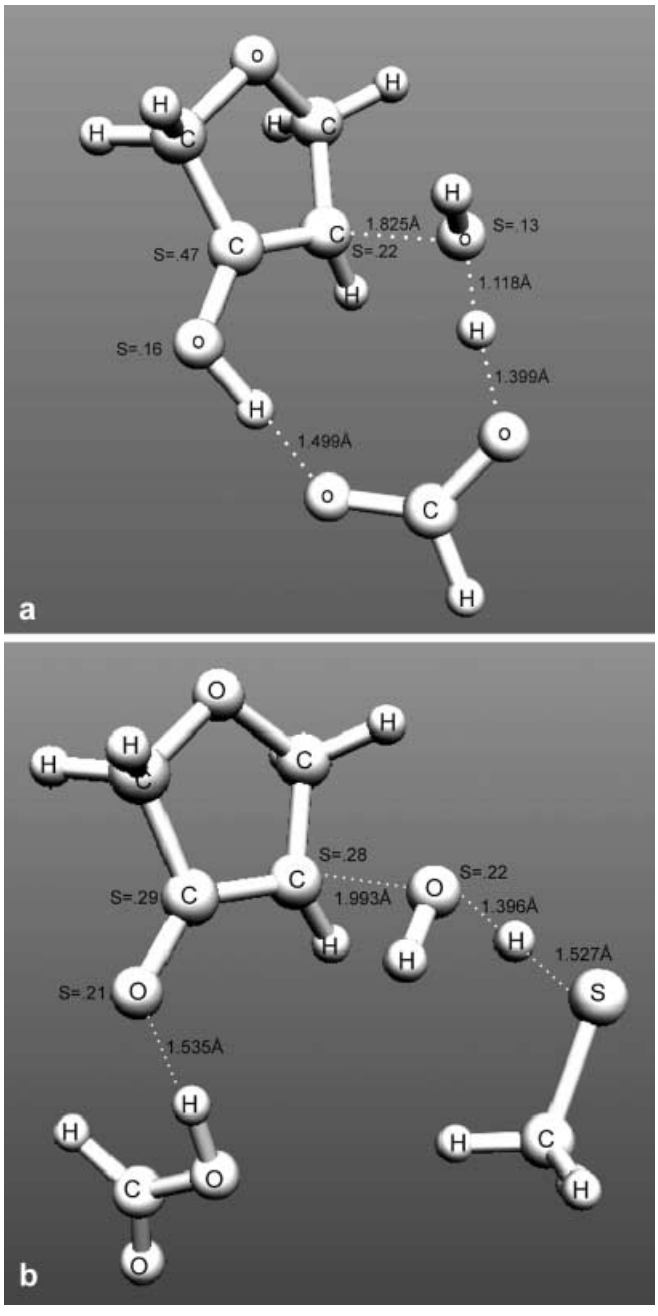


**Fig. 4. a** Optimized geometry of **a** the transition state for the 2→3 hydrogen transfer, catalyzed by a protonated glutamate, and **b** optimized geometry of the transition state for reaction 4, simultaneously catalyzed by a basic glutamate and an acid cysteine. Relevant *distances* (Å) and *spin densities* (a.u.) are indicated

assumption of using only neutral models in the active site. Here such a constraint was not imposed, and we have included charged species in the model when appropriate to the mechanisms being studied. This is justified by the fact that the RNR active site is not buried, having instead a very large cavity that accommodates a charged substrate. Furthermore, an anionic/radical disulfide has been detected by electron paramagnetic resonance at the active site [60], providing further evidence that charged species are present at the RNR active site. Other observations also

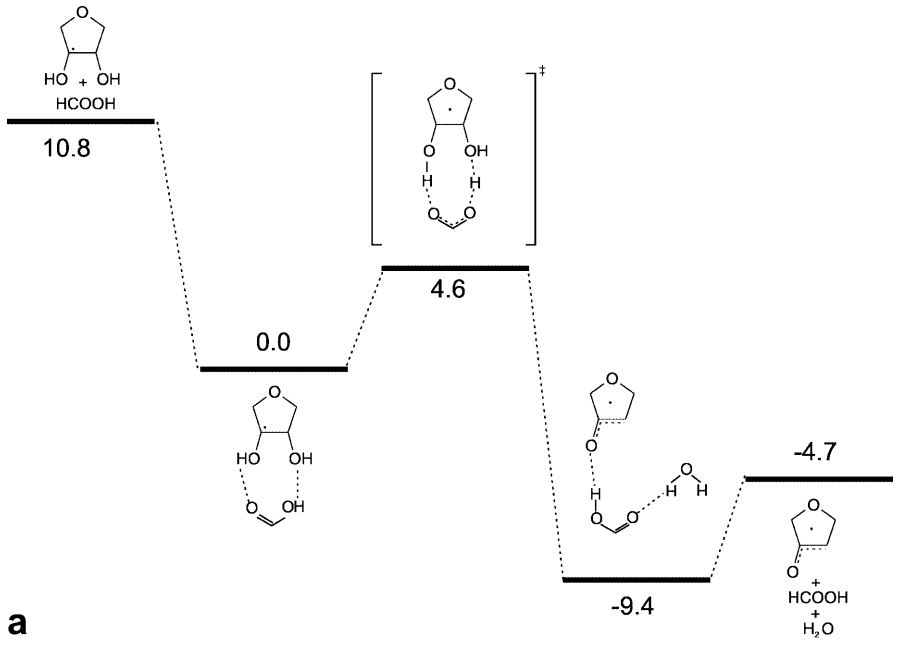


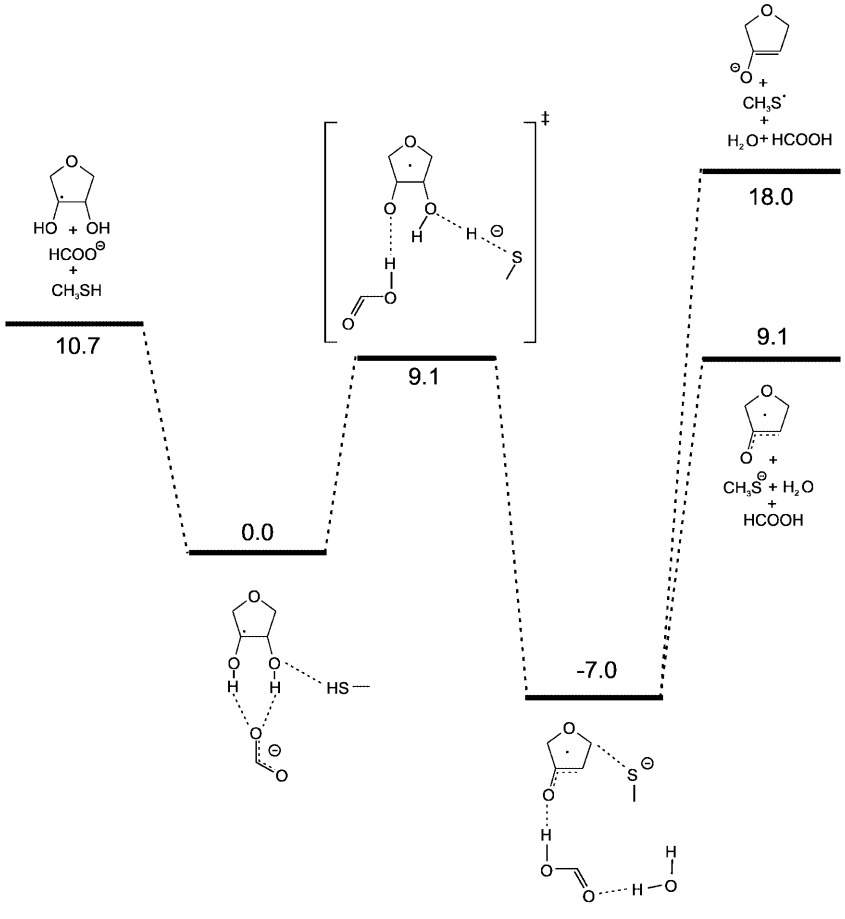


**Scheme 5. a** Activation energies and reaction enthalpies for the hydrogen transfer catalyzed by a protonated glutamate side chain, acting as a bifunctional catalyst. All energies in kcal $mol^{-1}$. **b** Activation energies and reaction enthalpies associated with the reaction step illustrated in Scheme 1. All energies in kcal $mol^{-1}$

suggest that neutral models might be inadequate to reproduce the active site of this enzyme. Persson et al. [56] measured the pH dependence of the enzyme activity. They concluded that the reaction rate increases with an increase of the pH from 6 to 8, the latter being the optimal value for catalysis. In the experiments of Lenz and Giese, the same was also observed [27]. However, the hypothesis of catalysis using a protonated glutamate is incoherent with that observation, as an increase in the pH favors the unprotonated form of the glutamate. Moreover, the

**Table 1.** Activation energies and reaction enthalpies at 298 K and 1 bar for all the chemical reactions studied in the present work. For each reaction the results obtained with the three theoretical levels employed are discriminated: 6-31G(d) (*MB*), 6-311 + G(2d,p) (*LB*), 6-311 ++ G(3df,3pd) (*VLB*). All energies in kcal $mol^{-1}$

| Reaction | Basis set | $E_a$ | $\Delta H_R$ |
|---|---|---|---|
| Base catalysis – deprotonation | MB | 21.2 | 14.5 |
| | LB | 22.4 | 14.5 |
| | VLB | 22.6 | 14.9 |
| Base catalysis – protonation by Cys225 | MB | 1.4 | −22.7 |
| | LB | 1.6 | −21.7 |
| | VLB | 2.1 | −21.4 |
| Base catalysis – protonation by Glu441 | MB | 4.0 | −16.3 |
| | LB | 1.3 | −19.9 |
| | VLB | 1.3 | −20,0 |
| 1,2 hydroxyl shift | MB | 24.0 | −0.7 |
| | LB | 21.0 | 0.0 |
| | VLB | 20.0 | −1.1 |
| Acid and base catalysis by Glu441v | MB | 6.1 | −5.4 |
| | LB | 4.0 | −9.8 |
| | VLB | 4.6 | −9.4 |
| Acid catalysis by Cys225 and base catalysis by Glu441 | MB | 12.9 | −2.6 |
| | LB | 8.7 | −6.9 |
| | VLB | 9.1 | −7.0 |

reaction rate should not be affected by changing the pH if only neutral residues were present at the active site.

The intrinsic $pK_a$ value for the glutamate side chain corresponds to 4.3 [58]. The $pK_a$ of the Glu441 side chain in the RNR active site should be very close to that, since no specific interactions that favor the protonated or the unprotonated form of the side chain carboxylate group are present. So, at physiological pH, only one in each around 502 glutamates will be protonated.

We may thus conclude that this mechanism does occur if the Glu441 side chain is protonated at the moment of the enzyme–substrate complex formation. However, owing to the pH dependence, the mechanism cannot justify, on its own, the overall catalytic activity of the RNRs. Therefore, there ought to be an alternative way for the majority of cases, where the Glu441 side chain is unprotonated.

One mechanism that can occur when the Glu441 side chain is unprotonated corresponds to the abstraction of the 3′ hydroxyl hydrogen simultaneously with the protonation of the 2′ hydroxyl oxygen. Stubbe and van der Donk [1] proposed such a mechanistic step in their latest postulated catalytic cycle (Scheme 1). We here assume that the basic catalyst is Glu441 and the acid catalyst is Cys225. The crystallographic structure of the enzyme with the bound substrate shows that both of them occupy very good positions to participate in the reaction. The oxygen of the Glu441 side chain is at hydrogen-bonding distance from the 3′ hydroxyl group and the Cys225 thiol group is at hydrogen-bonding distance from the 2′ hydroxyl group. The results of our computational study of this system can be summarized as follows. In the reactants one carboxylate oxygen forms hydrogen bonds with the two hydroxyl groups, with lengths of 1.633 and 1.710 Å, respectively. Simultaneously, the thiol group of the Cys225 amino acid forms a hydrogen bond with the 2′ oxygen, with a bond length of 1.990 Å. At the transition state (Fig. 4b), the proton of the 3′ hydroxyl group has already been abstracted by the glutamate, and participates in a short, strong hydrogen bond with the 3′ oxygen; bond length 1.535 Å. The 2′ C–O bond is very elongated (1.993 Å), and the hydroxyl group is already leaving the ribonucleotide. The proton of the thiol group makes a very short hydrogen bond with the 2′ hydroxyl group (1.396 Å), and the S–H bond of the cysteine is elongated (1.527 versus 1.364 Å in the reactants). In the reactants, the spin density is mainly localized at the 3′ carbon (0.93 a.u.), although the 3′ oxygen also exhibits appreciable spin density (0.13 a.u.). At the transition state, the spin density is shifted to the direction of the sulfur atom, and becomes almost evenly distributed between the 3′ oxygen (0.21 a.u.), the 3′ carbon (0.29 a.u.), the 2′ carbon (0.28 a.u.) and the 2′ oxygen (0.22 a.u.). In the products, the spin density becomes mainly localized at the sulfur atom (0.51 a.u.), but the 3′ oxygen and the 2′ carbon still retain some spin density (0.10 and 0.22 a.u., respectively). The charge distribution is also shifted in the direction of the cysteine, i.e. the negative charge that was concentrated at the glutamate in the reactants (−1.08 a.u.) becomes almost evenly shared between the cysteine and the 2′-deoxy-3′-ketonucleotide moiety (−0.45 and −0.53 a.u., respectively).

The activation energies and reaction enthalpies for the reaction are depicted in Scheme 5b. The reaction has an activation energy of 9.1 kcal $mol^{-1}$ and a reaction energy of −7.0 kcal $mol^{-1}$. Zero-point and thermal corrections account for a decrease of 5.5 kcal $mol^{-1}$ in the activation energy and 2.5 kcal $mol^{-1}$ in the reaction enthalpy.

The long-range polarization accounts for a decrease of 1.4 kcal $mol^{-1}$ in the reaction barrier and 0.2 kcal $mol^{-1}$ in the reaction enthalpy. Geometry changes induced by the dielectric medium are small. In the reactants there is a shortening of 0.036 Å in the hydrogen bond between the thiol and the 2′ hydroxyl groups. At the transition state, the hydrogen bond between the protonated side chain of the glutamate and the 3′ oxygen is shortened by 0.035 Å by the continuum. The distance between the 2′ hydroxyl group (leaving the ring) and the 2′ carbon in the ribonucleotide is also shortened by

0.057 Å. The hydrogen bond between the thiol and the 2′ hydroxyl groups follows the same trend, being shortened by 0.055 Å in the protein environment. The influence of the surrounding continuum on the zero-point and thermal energies corresponds to a decrease of 2.0 kcal $mol^{-1}$ in the activation energy and of 1.9 kcal $mol^{-1}$ in the reaction enthalpy.

This simultaneous acid- and base-catalyzed mechanism fits the observed kinetics of the catalytic process [56]. It is also strongly supported by the X-ray crystallographic structure of the enzyme–substrate complex [37], and takes into account the physiological protonation states of the amino acids involved at the active site. The results obtained point to this mechanism as the one occurring when the key active-site Glu441 amino acid is in its unprotonated form.

Finally, we must determine in which fragment the radical will be localized. Calculating the difference in energy between the monomers that participate in the reaction shows that placing the radical at the 2′-deoxy-3′-ketonucleotide moiety and the negative charge at the cysteine thiolate results in a larger stabilization (by 8.9 kcal $mol^{-1}$) than placing the radical and charge at the opposite species. Therefore, we may conclude that after the complex between the products is separated, the radical becomes localized at the 2′-deoxy-3′-ketonucleotide and that the cysteine retains a negative charge. This corresponds to a similar situation as observed in reaction 1b. In addition, the anionic Cys225 is ready to form the reduced disulfide bridge to Cys462, via a disulfide radical anion intermediate, as postulated by Stubbe and van der Donk [1], and observed a posteriori experimentally, both by electron paramagnetic resonance and X-ray crystallography methods [37, 61].

## 4 Conclusions

In this work we have studied the mechanism of dehydration of ribonucleotides assisted by the enzyme RNR. We have explored from a theoretical point of view the current working hypotheses, as well as alternative catalytic pathways proposed herein. The activation energies and reaction enthalpies at 298 K are presented in Table 1.

The results are compared with the available experimental data, namely the observed kinetics of dehydration [56], the crystallographic structure of the enzyme with the bound substrate [37], the pH dependence of the enzymatic activity [56], as well as data from similar chemical reactions [27, 46]. It is concluded that dehydration occurs via two different acid-/base-catalyzed mechanisms. The first uses a protonated glutamate as a bifunctional catalyst, and has a very low activation energy. [31]. On the basis of previous theoretical results this mechanism would be the most favorable one. However, this should only occur in a reduced number of cases, since the relative abundance of the protonated glutamates at physiological pH corresponds to about 0.2% only. The second mechanism assumes that an unprotonated glutamate acts as a base, and simultaneously a cysteine thiol group acts as an acidic catalyst. This mechanism should occur in the majority of cases, where the glutamate exists in the unprotonated form. It is strongly supported by the X-ray crystallographic structure, and all residues employed are in their natural protonation states.

The results also allow us to clarify some aspects concerning the role played by the enzyme during the reaction, and to understand how enzymes contribute to such high reaction rates relative to similar processes in the aqueous phase. The influence of the surrounding medium on the optimized geometries and reaction energies is small, and the calculations show that its inclusion is not capable of inverting the relative feasibility of the two hypothetical mechanisms, or even to change the acceptance or rejection of a given mechanism. In other words, its contribution to the rate acceleration is not important. This means that this enzyme cannot make a differential stabilization of the transition states in relation to the reactants via long-range interactions. On the other hand, in the aqueous phase, trimolecular reactions, such as the last acid- and base-catalyzed dehydration, are highly improbable, since the probability of all the reactants to spontaneously generate a productive geometry is very small. However, at the enzyme active site, the binding of the substrate and the configuration of the amino acids provide optimal conditions. The role of the enzyme is hence to orient all reactants in a favorable geometry, thereby promoting a rate acceleration.

*Acknowledgements.* Fundação para a Ciência e Tecnologia (project POCTI/35736/99, Portugal), the National Foundation for Cancer Research (USA) and the Swedish Science Research Council (LAE) are gratefully acknowledged for financial support.

## References

1. Stubbe J, van der Donk WA (1998) Chem Rev 98: 705
2. Eriksson S, Sjöberg B-M (1989) In: Hervé G (ed) Allosteric enzymes. CRC, Boca Raton, p 189
3. Stubbe J (1990) Adv Enzymol Relat Areas Mol Biol 63: 349
4. Reichard P (1993) Science 260: 1773–1777
5. Stubbe J, van der Donk WA (1995) Chem Biol 2: 793
6. Sjöberg B-M (1995) In: Eckstein F, Lilley D (eds) Nucleic acids and molecular biology, vol 9. Springer, Berlin Heidelberg New York, p 192
7. Cory JG, Chiba P (1989) In: Cory JG, Cory AH (eds) Combination chemotherapy directed at the components of nucleoside diphosphate reductase. Pergamon, New York, p 245
8. Robins MJ, Samano MC, Samano V (1995) Nucleosides Nucleotides 14: 485
9. Nocentini J (1996) Crit Rev Oncol Hematol 22: 89
10. Gerfen GJ, van der Donk WA, Yu G, McCarthy JR, Jarvi ET, Matthews DP, Farrar C, Griffin RG, Stubbe J (1998) J Am Chem Soc 120: 3823
11. McCarthy JR, Sunkara PS (1995) In: Weiner DB, Williams WB (eds) Design, synthesis and anti-tumor activity of an inhibitor of ribonucleotide reductase. CRC, Boca Raton, pp 3–32
12. McCarthy JR, Sunkara PS, Matthews DP, Bitonti AJ, Jarvi ET, Sabol JS, Resvick RJ, Hubber EW, van der Donk WA, Yu G, Stubbe J (1996) ACS Symp Ser 639: 246
13. Bitonti AJ, Dumont JA, Bush TL, Cashman EA, Crossdoersen DE, Wright PS, Matthews DP, McCarthy JR, Kaplan DA (1994) Cancer Res 54: 1485
14. Bitonti AJ, Bush TL, Lewis MT, Sunkara PS (1995) Anticancer Res 15: 1179
15. Hammersten E, Reichard P, Saluste E (1950) J Biol Chem 183: 105

16. Reichard P, Estborn B (1951) J Biol Chem 188: 839
17. Blackley RL, Barker HA (1964) Biochem Biophys Res Commun 16: 391
18. Beck HS, Hardy J (1965) Proc Natl Acad Sci USA 54: 286
19. Barlow T (1988) Biochem Biophys Res Commun 155: 747
20. Fontecave M, Eliasson R, Reichard P (1989) Proc Natl Acad Sci USA 86: 2147
21. Schimpff-Weiland G, Follman H, Auling G (1981) Biochem Byophys Res Commun 102: 1276
22. Willing A, Follman H, Auling G (1988) Eur J Biochem 178: 603
23. Griepenburg U, Lassman G, Auling G (1996) Free Rad Res 26: 473
24. Reichard P (1993) Science 260: 1773
25. Siegbahn PEM, Eriksson L, Himo F, Pavlov M (1998) J Phys Chem B 102: 10622
26. Mohr M, Zipse H (1999) Chem Eur J 5: 3046
27. Lenz R, Giese B (1997) J Am Chem Soc 119: 2784
28. Sjöberg B-M (1997) Struct Bonding 88: 139
29. Lammers M, Follman H (1983) Struct Bonding 54: 27
30. Nordlund P, Eklund H (1993) J Mol Biol 232: 123
31. Siegbahn P (1998) J Am Chem Soc 120: 8417
32. Zipse H (1995) J Am Chem Soc 117: 11798
33. Licht S, Stubbe J (1998) In: Poulter CD (ed) Comprehensive natural products chemistry. Elsevier, New York, pp
34. Licht S, Stubbe J (1999) In: Bartons SD et al (eds) Comprehensive natural products chemistry, vol 5. Elsevier, New York, p 163
35. Stubbe J, Ge J, Yee C (2001) Trends Biochem Sci 26: 93
36. Cho K, Himo F, Graslund A, Siegbahn PEM (2001) J Phys Chem B 105: 6645
37. Eriksson M, Uhlin U, Ramaswamy S, Ekberg M, Regnström K, Sjöberg B-M (1997) Struct Bonding 5: 1077
38. Himo F, Siegbahn PEM (2000) J Phys Chem B 104: 7502
39. Robins MJ, Guo Z, Samano MC, Wnuk SF (1999) J Am Chem Soc 121: 1425
40. Beckwith ALJ, Crich D, Duggan PJ, Yao Q (1997) Chem Rev 97: 3273
41. Stubbe J (1990) J Biol Chem 265: 5329
42. Beckwith ALJ, Crich D, Duggan PJ, Yao Q (1997) Chem Rev 97: 3273
43. Stubbe J (1990) J Biol Chem 265: 5329
44. Smith DM, Stacey DW, Wetmore SD, Radom L (2001) In: Eriksson LA (ed) Theoretical biochemistry – Processes and properties of biological systems. Elsevier, Amsterdam, p 183, and references therein
45. Smith DM, Golding BT, Radom L (1999) J Am Chem Soc 121: 5700
46. George P, Glusker JP, Bock CW (1997) J Am Chem Soc 119: 7065, and references therein
47. Becke AD (1993) J Chem Phys 98: 5648
48. Lee C, Yang W, Parr R (1998) J Phys Rev B 37: 785
49. Hertwig RW, Koch W (1995) J Comput Chem 16: 576
50. Forrester J, Frisch Æ (1996) In: Exploring chemistry with electronic structure methods. Gaussian, Pittsburgh, pp 64, 157
51. Himo F, Eriksson LA (2001) In: Eriksson LA (ed) Theoretical biochemistry – Processes and properties of biological systems. Elsevier, Amsterdam, p 149
52. Siegbahn PEM (1996) J Phys Chem 100: 14672, and references therein
53. Frisch MJ, Trucks GW, Schlegel HB, Scuseria GE, Robb MA, Cheeseman JR, Zakrzewski VG, Montgomery JA Jr, Stratmann RE, Burant JC, Dapprich S, Millam JM, Daniels AD, Kudin KN, Strain MC, Farkas O, Tomasi J, Barone V, Cossi M, Cammi R, Mennucci B, Pomelli C, Adamo C, Clifford S, Ochterski J, Petersson GA, Ayala PY, Cui Q, Morokuma K, Malick DK, Rabuck AD, Raghavachari K, Foresman JB, Cioslowski J, Ortiz JV, Baboul AG, Stefanov BB, Liu G, Liashenko A, Piskorz P, Komaromi I, Gomperts R, Martin RL, Fox DJ, Keith T, Al-Laham MA, Peng CY, Nanayakkara A, Challacombe M, Gill PMW, Johnson B, Chen W, Wong MW, Andres JL, Gonzalez C, Head-Gordon M, Replogle ES, Pople JA (1998) Gaussian 98, revision A.9. Gaussian, Pittsburgh PA
54. Blomberg MRA, Siegbahn PEM, Babcock GT (1998) J Am Chem Soc 120: 8812
55. Mulliken RS (1955) J Chem Phys 23: 1833
56. Persson A, Eriksson M, Katterle B, Pötsch S, Sahlin M, Sjöberg, -M (1997) J Biol Chem 272: 31533
57. Mohr M, Zipse H (2001) Phys Chem Chem Phys 3: 1246
58. Greighton T (1993) Proteins: structures and molecular properties. Freeman, New York.
59. Smith DM, Golding BT, Radom L (2001) J Am Chem Soc 123: 1664
60. Eriksson M, Uhlin U, Ramaswamy S, Ekberg M, Regnstrom K, Sjoberg B-M, Eklund H (1997) Structure 5: 1077
61. Lawrence CC, Bennati M, Obias HV, Bar G, Griffin RG, Stubbe J (1999) Proc Natl Acad Sci USA 96: 8979